Bioactive Materials 5 (2020) 286–296

Contents lists available at ScienceDirect

Bioactive Materials

journal homepage: http://www.keaipublishing.com/biomat

# A microarray platform designed for high-throughput screening the reaction conditions for the synthesis of micro/nanosized biomedical materials

Xiaoyu Li[a,b,c,d,e], Xiran Yang[a,b,c,d,e], Lei Liu[a,b,c,d,e], Peipei Zhou[f], Jianhua Zhou[f,***], Xuetao Shi[a,b,c,d,e,**], Yingjun Wang[a,b,c,d,e,*]

[a] School of Materials Science and Engineering, South China University of Technology, Guangzhou, 510640, PR China
[b] National Engineering Research Center for Tissue Restoration and Reconstruction, South China University of Technology, Guangzhou, 510006, PR China
[c] Key Laboratory of Biomedical Engineering of Guangdong Province, South China University of Technology, Guangzhou, 510006, PR China
[d] Key Laboratory of Biomedical Materials and Engineering of the Ministry of Education, South China University of Technology, Guangzhou, 510006, PR China
[e] Innovation Center for Tissue Restoration and Reconstruction, South China University of Technology, Guangzhou, 510006, PR China
[f] School of Engineering, Sun Yat-sen University, Guangzhou, 510275, PR China

ARTICLE INFO

*Keywords:*
Microfluidics
High-throughput
Concentration gradient
Calcium phosphates

ABSTRACT

Materials research usually relies on lengthy and largely trial-and-error methods, high-throughput technology has thereby emerged as an alternative method which is proven to be a simple, rapid, accurate and sensitive technique. Here, we presented a microfluidic platform with a set of 6 × 6 microarray chips for high-throughput synthesis and rapid screening the reaction conditions of biomedical materials. The core design of this platform is to generate concentration gradient inside microarray chips. Considering that calcium phosphates (CaP) are the most important inorganic constituents of biological hard tissues, different phases of calcium phosphates particles were synthesized with various morphogenesis when the reaction conditions such as Ca/P concentration ratio, NaOH concentration were screened using our platform. And this platform is universal and expected to apply to other systems for high-throughput screening and synthesis.

## 1. Introduction

In a general synthesis process of biomedical materials, researchers usually draw on previous experience or others work from published papers to adjust their own experimental parameters and expectations for the desired results [1]. This trial-and-error method is obviously very time and funding consuming [2,3]. In addition, it is common that researchers around the world execute diverse synthetic methods to obtain the same sample, and they usually focus on a single aspect and neglect profound and systematic research, which is a huge waste of resources. Additionally, with technological development, this method that requires a long R&D cycle will lead to obsoletion [1].

High-throughput technology has thereby emerged in this context [4–7]. This technique involves parallel synthesis and characterization of materials, leading to minimized product development cycles, quickly attainable results, an increase in research efficiency, workflow optimization and accelerated innovation [8,9]. Many remarkable achievements have been made in recent decades, for instance, the platform designed to run automation-friendly coupling reactions to resize the screening of over 1500 reactions per day using only 0.02 mg of material per reaction [10] or the platform for automated nanomole-scale reaction screening produced by Pfizer, which allows the generation of liquid chromatography-mass spectrometry data for 5760 reactions per day [11]. However, these platforms also require large-scale high-throughput facilities and have large burdens in terms of placement and maintenance, which are unaffordable for most labs [12]. Microfluidic technology is, on the other hand, a rapid, reliable and cost-effective method which provides a powerful tool for screening biomedical materials on a single microchip with little reagents at defined time [13–15]. Miniaturizing the many thousands of assay reactions and replacing robotic automation with integrated microfluidic handling aim to deliver a powerful, unbiased mode of discovery [12,16]. The small

Peer review under responsibility of KeAi Communications Co., Ltd.
* Corresponding author. School of Materials Science and Engineering, South China University of Technology, Guangzhou 510640, PR China.
** Corresponding author. School of Materials Science and Engineering, South China University of Technology, Guangzhou 510640, PR China.
*** Corresponding author. School of Engineering, Sun Yat-sen University, Guangzhou 510275, P. R. China.
*E-mail addresses:* joylixiaoyu1992@163.com (X. Li), yangxiran813@163.com (X. Yang), 1097221497@qq.com (L. Liu), peip.zhou@foxmail.com (P. Zhou), zhoujh33@mail.sysu.edu.cn (J. Zhou), shxt@scut.edu.cn (X. Shi), imwangyj@163.com (Y. Wang).

https://doi.org/10.1016/j.bioactmat.2020.02.003
Received 31 December 2019; Received in revised form 3 February 2020; Accepted 3 February 2020

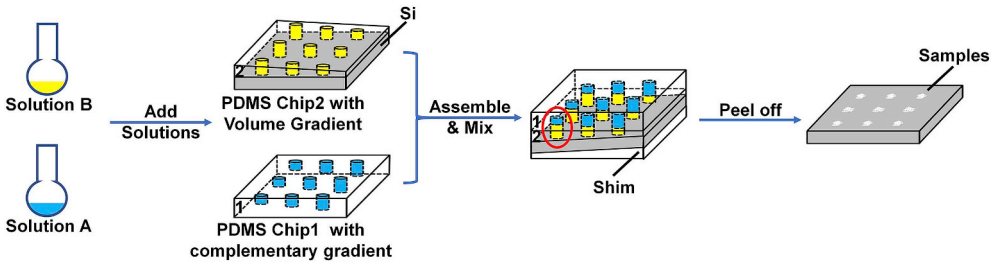


**Fig. 1.** Schematic overview of fabricating microreactors on a silicon substrate: PDMS chip1 with partially perforated holes and PDMS chip2 with fully perforated holes fixed on a silicon substrate; a reactant solution was added into PDMS chip1, while another reactant solution was added into PDMS chip2; the reaction was initiated immediately after mixing of the solutions in the contact holes from the opposing PDMS chips (the deepest holes in PDMS chip1 aligned with the shallowest holes in PDMS chip2); a precipitated product array could be found on the silicon substrate after reaction.

volume of the microchip results in a remarkable saving of chemicals and an efficient way to save time [17,18]. As for microarray chips, the in-situ reaction synthesis enables rapid mixing of reagents and accurate determination of experimental conditions.

Calcium phosphates (CaP) are the most important inorganic constituents of biological hard tissues such as bones and teeth [19,20], the properties of good biocompatibility, bioactivity, biodegradability and convenience for surface modification allow CaP to be an intriguing topic in biomedical areas such as gene delivery and tissue engineering [21] and these properties are highly influenced by the micro/nanostructure of calcium phosphates. In this paper, a 6 × 6 microarray platform was designed and parallel experiments with similar reaction conditions can be carried out on this platform simultaneously, while a specific parameter of concern varies in broad range which could produce a series of aiming samples for screening in a single experiment. And we used this designed platform for rapid screening of the experimental conditions pivotal to the production of micro/nanosized calcium phosphates particles, stable and calculable gradients of Ca/P concentration ratio and NaOH concentration were generated by adding solutions into polydimethylsiloxane (PDMS) chips with different hole depths. This technique helps to quickly identify the condition range for generating CaP structures with specific morphologies and guiding for the high-volume production with optimized reaction conditions.

## 2. Materials and methods

### 2.1. Chemicals and materials

Calcium nitrate tetrahydrate [$Ca(NO_3)_2{\cdot}4(H_2O)$] and ammonium phosphate dibasic [$(NH_4)_2HPO_4$] were both purchased from Sigma–Aldrich and used as received. Sodium hydroxide (NaOH, 3.57 M) was purchased from Aladdin. Lemon and brilliant blue mixed colors were obtained from Shanghai Dyestuffs Research Institute Co., Ltd. Polydimethylsiloxane (PDMS) prepolymer (Dowsil TM 184 silicone elastomer kit) was obtained from Dow Europe GmbH. The water used in all reactions was deionized water.

### 2.2. Fabrication of the screening chip

PDMS chip1 and chip2 were fabricated by molding against a metal mold with a 6 × 6 micropillar array, and the diameter of the micropillars was 1 mm, while the heights of the micropillars increased from 500 μm to 2500 μm with a 400 μm height difference between two adjacent pillars (the heights of the micropillars in each column were 500, 900, 1300, 1700, 2100 and 2500 μm, and the heights of the micropillars in each row were the same). PDMS chip3 and chip4 were fabricated by molding against another metal mold with a location-matched 6 × 6 micropillar array, while the diameter and height of the micropillars were both 1500 μm. The angle between the upper section of the pillars and the horizontal plane was approximately 3.81°, and the distance between the centers of two adjacent pillars was 6 mm.

A mixture (uncured PDMS) of a silicon elastomer base and a curing agent at a certain ratio (= 12:1 *w/w*) was prepared and degassed before being poured into a clean culture dish with a metal mold and a silicon substrate as displayed in Figs. S1 in the Supplementary Information. For PDMS chip1 and PDMS chip3 with partially perforated holes, molding I required that the poured uncured PDMS cover the top edge of the metal mold base before degassing; for molding II, over approximately 2 mm of uncured PDMS should cover the metal mold before vacuuming. As for PDMS chip2 and chip4 with fully perforated holes, a silicon substrate (40 × 40 × 0.725 $mm^3$) was also necessary during the manufacture process. In molding I, the poured uncured PDMS should be enough to cover the whole silicon substrate; after vacuuming for approximately 15 min, more uncured PDMS was required to cover the lower edge of the metal mold base in molding II before degassing. For all the uncured PDMS chips, a heating process (65 °C in a drying oven for 2 h) was executed after degassing, and then, after cutting off the superfluous cured PDMS, the desired PDMS chips were preserved in sealed clean culture dishes prior to use. Photographs of PDMS chip1 (left) and chip2 (right) are displayed in Fig. S1 in the Supplementary Information and design drawing of flipped over PDMS chip1 fixed on a PMMA block, with PDMS chip2 fixed on a silicon substrate at the bottom is displayed in Fig. S1 in the Supplementary Information.

### 2.3. Generation of reagent concentration gradient

In this screening platform, the core design is to generate a concentration gradient by mixing solutions with different volumes, and a series of mixed solutions with different reactant concentrations thereby emerged in the microreactors (as shown in Fig. 1). The reactant concentration in each microreactor could be determined by calculation. A colorant mixing experiment (shown in Fig. S2 in the Supplementary Information) was carried out to obtain a visible and intuitive gradient formation result by adding 1 g/L brilliant blue pigment into PDMS chip1 and adding lemon pigment with the same mass concentration into PDMS chip2; a plasma treatment for 3 min should be implemented before adding any solutions due to the hydrophobic surface of the PDMS chips so that the solution could flow into the holes of the PDMS chips. We used 1 mL syringes to remove the air bubbles inside the holes and filter paper to absorb extra solution on the surface of the PDMS chips. Furthermore, the metal molds used for fabrication of PDMS chips were manufactured according to the same CAD drawing so that the holes in the PDMS chips could be precisely aligned, and as a result, sealed microreactors were generated. After merging PDMS chip1 and PDMS chip2 (the deepest holes in PDMS chip1 aligned with the shallowest holes in PDMS chip2), the combined PDMS chips were left standing for 2 h at room temperature to ensure complete diffusion between the color solutions.

Because of the difficulties of precise manual alignment of matching holes, we also designed a support system that contained a plastic base with a lug boss (4 × 4 × 0.1 $cm^3$), an outer square frame (inner dimensions 4 × 4 × 2.5 $cm^3$) and a locator (4 × 4 × 0.5 $cm^3$) that

possessed four cylinders (ϕ = 0.9 mm; H = 0.5 mm) with positions matched to those of the micropillars on the metal molds at the four corners. By locating the PDMS chip on the locator and pressing the locator inside the square frame while a silicon substrate or a PMMA block (4 × 4 × 0.5 $cm^3$) with a smooth surface was placed on the lug boss of the plastic base, we could adhere the PDMS chip on the silicon or PMMA block at a specific location as well as the hole-array on the PDMS chip. The support system was also indispensable during the mixing and reaction process to ensure that the holes of the opposing PDMS chips were matched, as shown in Fig. S1 and Fig. S2 in the Supplementary Information. A weight (500 g) was placed on the PMMA block to ensure better contact between the PDMS chips.

### 2.4. High-throughput screening of the concentrations of reactants for calcium phosphates synthesis

By placing PDMS chip1 on the locator and pressing the other side of the locator inside the square frame fixed on the plastic base with a PMMA block on the lug boss, PDMS chip1 could be fixed on the PMMA block. PDMS chip2 could be fixed on a silicon substrate through the same procedure. After treatment with plasma for 3 min, a 0.06 M $(NH_4)_2HPO_4$ solution was added to PDMS chip2, while a 0.06 M Ca $(NO_3)_2$ solution was added to PDMS chip1. 1 mL syringes were used to remove the air bubbles inside the holes, and filter paper was used to remove extra solution on the surface of the PDMS chips. First, PDMS chip2 fixed on the silicon substrate containing the $(NH_4)_2HPO_4$ solution was placed on the lug boss inside the square frame. Then, PDMS chip1 fixed on the PMMA block containing the $Ca(NO_3)_2$ solution was quickly flipped over in the right direction so that the deepest holes in PDMS chip1 aligned with the shallowest holes in PDMS chip2, and the PMMA block was pressed into the square frame (thereby establishing a horizontal $C_{Ca}/C_P$ concentration ratio gradient; $C_{Ca}/C_P$ = 2.5/0.5; 2.1/0.9; 1.7/1.3; 1.3/1.7; 0.9/2.1; and 0.5/2.5). The entire system was wrapped in preservative film and placed on a shaking table at 37 °C to obtain a better mixing effect, while a weight (500 g) was placed on the PMMA block to ensure better contact between the PDMS chips. The reaction was triggered immediately after the two solutions came into contact, and calcium phosphates began to form. After 24 h, the entire system was removed from the shaking table, the preservative film was removed, and the system was placed into a vacuum drying oven for drying. Then, the entire system was soaked in deionized water for 3 days, and the deionized water was changed per day to remove soluble impurities. Then, the PDMS chips were peeled off, and the formed calcium phosphates structure was left at the generation positions on the silicon substrate for SEM and other characterization.

In the initial experiment, we built a horizontal concentration ratio gradient ($C_{Ca}/C_P$ = 0.5/2.5; 0.9/2.1; 1.3/1.7; 1.7/1.3; 2.1/0.9; and 2.5/0.5). We also demonstrated an orthogonal $C_{Ca}/C_P$ concentration ratio gradient, as listed in Table 1. To manipulate the concentration ratio gradient, after adding 0.06 M $(NH_4)_2HPO_4$ to PDMS chip2 and 0.06 M $Ca(NO_3)_2$ to PDMS chip1, PDMS chip1 fixed on the PMMA block was quickly flipped over in a specific direction so that the end of PDMS chip1 with the deepest holes aligned with the deepest holes in PDMS chip2 and the other end of PDMS chip1 with the deepest holes aligned with the shallowest holes in PDMS chip2, and vice versa. Then, the PMMA block was pressed into the square frame. Except for the opposing PDMS chip alignment direction, the rest of the procedures were the same as in the preliminary experiment.

### 2.5. Scale-up experiments for calcium phosphates synthesis according to screening results

The scale-up experiments were carried out based on the initial experimental conditions; the reaction volume was increased from $V_0$ = 2.355 μL to V = 15 μL ($V/V_0 \approx 6.37$). We also took solvent evaporation during the reaction into consideration, and the concentrations of both reactants were increased by six times ($C_{Ca} = C_P$ = 0.36 M) in the scale-up experiments. Briefly, $V_{Ca}$ μL of a 0.36 M Ca $(NO_3)_2$ solution was added into 0.5 mL EP tubes containing $V_P$ μL of a 0.36 M $(NH_4)_2HPO_4$ solution, and the volume ratio between the two solutions in each scale-up experiment was matched to the volume ratio between the two solutions in the chip screening experiment ($V_{Ca} + V_P$ = 15 μL: $V_{Ca1}$ = 12.5 μL, $V_{P1}$ = 2.5 μL, $V_{Ca1}/V_{P1}$ = 2.5/0.5; $V_{Ca2}$ = 10.5 μL, $V_{P2}$ = 4.5 μL, $V_{Ca2}/V_{P2}$ = 2.1/0.9; $V_{Ca3}$ = 8.5 μL, $V_{P3}$ = 6.5 μL, $V_{Ca3}/V_{P3}$ = 1.7/1.3; $V_{Ca4}$ = 6.5 μL, $V_{P4}$ = 8.5 μL, $V_{Ca4}/V_{P4}$ = 1.3/1.7; $V_{Ca5}$ = 4.5 μL, $V_{P5}$ = 10.5 μL, $V_{Ca5}/V_{P5}$ = 0.9/2.1; $V_{Ca6}$ = 2.5 μL, $V_{P6}$ = 12.5 μL, $V_{Ca6}/V_{P6}$ = 0.5/2.5). The reaction tubes were placed on a shaking table at 37 °C for 24 h, after which the supernatant liquid in the EP tubes was removed, and the precipitates were washed and dispersed by deionized water, then dripped on filter paper to remove soluble impurities and air dried. The dried precipitates were collected for SEM and other characterization.

### 2.6. High-throughput screening the concentration of additive reagent for calcium phosphates synthesis

To introduce multiple reagents into the research, we also designed another metal mold to fabricate PDMS chip3 and chip4, in which the holes had a uniform depth (1500 μm), as mentioned earlier. Fig. 5 shows a schematic of the general procedure for the application of this platform to additive agent concentration screening. By placing PDMS chip1 on the locator and pressing the other side of the locator inside the square frame fixed on the plastic base with a PMMA block on the lug boss, PDMS chip1 could be fixed on the PMMA block. PDMS chip3 was fixed on another PMMA block by the same method. The chips were both treated with plasma for 3 min, and then, a 0.06 M $(NH_4)_2HPO_4$ solution (pH adjusted to 4.51) was added into PDMS chip3, while a mixed solution contained 0.06 M $(NH_4)_2HPO_4$ and 0.070 M NaOH was added into PDMS chip1. 1 mL syringes were used to remove the air bubbles inside the holes, and filter paper was used to absorb extra solution on the surface of the PDMS chips. Then, PDMS chip3 fixed on one of the PMMA blocks was placed on the lug boss inside the square frame, and PDMS chip1 containing the mixed solution fixed on the other PMMA block was quickly flipped over and pressed into the square frame. The

**Table 1**
Microarray platform screening of an orthogonal $C_{Ca}/C_P$ concentration ratio gradient.

| $C_{Ca}/C_P$ | 1 | 2 | 3 | 4 | 5 | 6 |
|---|---|---|---|---|---|---|
| **A** | 2.5/0.5[a] | 2.5/0.9 | 2.5/1.3 | 2.5/1.7 | 2.5/2.1 | 2.5/2.5 |
| **B** | 2.1/0.5 | 2.1/0.9 | 2.1/1.3 | 2.1/1.7 | 2.1/2.1 | 2.1/2.5 |
| **C** | 1.7/0.5 | 1.7/0.9 | 1.7/1.3 | 1.7/1.7 | 1.7/2.1 | 1.7/2.5 |
| **D** | 1.3/0.5 | 1.3/0.9 | 1.3/1.3 | 1.3/1.7 | 1.3/2.1 | 1.3/2.5 |
| **E** | 0.9/0.5 | 0.9/0.9 | 0.9/1.3 | 0.9/1.7 | 0.9/2.1 | 0.9/2.5 |
| **F** | 0.5/0.5 | 0.5/0.9 | 0.5/1.3 | 0.5/1.7 | 0.5/2.1 | 0.5/2.5 |

[a] The boxed $C_{Ca}/C_P$ ratios match the $C_{Ca}/C_P$ ratios in the preliminary horizontal experiment.

[a]The boxed $C_{Ca}/C_P$ ratios match the $C_{Ca}/C_P$ ratios in the preliminary horizontal experiment.

whole system was wrapped in preservative film and left standing at room temperature for 2 h to ensure complete diffusion between the solutions, while a weight (500 g) was placed on the PMMA block to ensure better contact and sealing effect between the PDMS chips. Subsequently, PDMS chip4 was fixed on a silicon substrate using another support system and treated with plasma for 3 min. A 0.10 M $Ca(NO_3)_2$ solution was then added to PDMS chip4, 1 mL syringe was used to remove the air bubbles inside the holes, and filter paper was used to remove extra solution on the surface of the PDMS chip. Meanwhile, the preservative film wrapped around the support system was removed, and the adhered PDMS chips were removed from the support system. Then, PDMS chip1 was peeled off from PDMS chip3. The holes in PDMS chip3 now contained a mixed solution with 0.06 M $(NH_4)_2HPO_4$ and a concentration gradient of NaOH solution (the NaOH concentration was 0.0175, 0.0263, 0.0325, 0.0372, 0.0408; and 0.0438 M from the holes contacting the 500 μm wells to the holes contacting the 2500 μm wells in PDMS chip1, and the NaOH concentration in each microreactor was determined by calculation). After that, PDMS chip4 containing the 0.10 M $Ca(NO_3)_2$ solution fixed on the silicon substrate was placed on the lug boss inside the square frame; then, PDMS chip3 containing a mixed solution of $(NH_4)_2HPO_4$ and a NaOH concentration gradient fixed on the PMMA block was quickly flipped over, and the PMMA block was pressed into the square frame. The whole system was then wrapped in preservative film and placed on a shaking table at 37 °C to obtain a better mixing effect, while a weight (500 g) was placed on the PMMA block to ensure better contact between the PDMS chips. The reaction was triggered immediately after the two solutions came into contact, and calcium phosphates began to form. After 24 h, the entire system was removed from the shaking table, the preservative film was removed, and the system was placed into a vacuum drying oven for drying. Then, the entire system was soaked in deionized water for 3 days, and the deionized water was changed per day to remove soluble impurities. Then, the PDMS chips were peeled off, and the formed calcium phosphates structure was left at the generation positions on the silicon substrate for SEM and other characterization. We also built another NaOH concentration gradient by adding a 0.06 M $(NH_4)_2HPO_4$ solution (pH adjusted to 7.00) into PDMS chip3, while a mixed solution containing 0.06 M $(NH_4)_2HPO_4$ and 0.225 M NaOH was added into PDMS chip1, and thereby, a small NaOH concentration gradient (0.0563, 0.0844, 0.1045, 0.1195, 0.1313; and 0.1406 M) was formed. The remaining procedures remained the same. The pH of the mixed 0.06 M $(NH_4)_2HPO_4$ and NaOH solution in separate holes was tested by a pH meter.

### 2.7. Characterization

SEM images of samples were taken by a MERLIN FE-SEM (field emission scanning electron microscope) from Carl Zeiss after the samples were coated with Pt for 60 s, and X-ray diffraction (XRD) results were obtained using an Empyrean (PANalytical B. V) with Cu Kα radiation (λ = 1.540598 nm), while the Fourier transform-infrared (FT-IR) spectra were characterized using the KBr direct compression method with a CCR-1Thermo Nicolet spectrometer.

## 3. Results

Fig. 1 presents the general procedure for the application of the designed platform to reactant concentration screening, and the fabrication process of the PDMS chips is shown in Fig. S1 in the Supplementary Information and introduced in detail in the materials and methods section. Briefly, two PDMS chips containing a cylindrical hole array with a depth gradient (the depths of the holes in each column were 500, 900, 1300, 1700, 2100 and 2500 μm and in each row were the same) were combined and adhered on a silicon substrate; therefore, a two-dimensional array of microreactors was formed. PDMS chip1 with partially perforated holes contained solution A ($C_{A0}$), while PDMS chip2 with fully perforated holes, which was fixed on a silicon substrate, contained solution B ($C_{B0}$); then, PDMS chip1 was quickly flipped over in the right direction so that the deepest holes in PDMS chip1 aligned with the shallowest holes in PDMS chip2 (as displayed in Fig. S1 in the Supplementary Information) and was placed on PDMS chip2. Upon mixing of the solutions in matched holes, the reaction was triggered immediately after the two solutions came into contact, and since there were depth differences between the holes, a horizontal concentration ratio gradient ($C_A/C_B$) formed (Fig. S2 in Supplementary Information). After the reaction, the precipitated target products were found on the silicon substrate at the corresponding microreactor position, which means that we could obtain a product array for SEM and other characterization. Furthermore, the reactant concentration could be determined by calculation according to the equation below:

$$C_X = d_X / (d_X + d_Y) \times C_{X0} \quad (1)$$

$C_X$ is the concentration of solution X in the microreactor; $d_X$ is the depth of the holes in the PDMS chip containing solution X, $d_Y$ is the depth of the holes in the PDMS chip containing solution Y, and $C_{X0}$ is the concentration of solution X initially added into the PDMS chip. For instance, the concentration of solution A was 1/6 $C_{A0}$ [$C_A$ = 500 μm/(500 + 2500 μm) $C_{A0}$], while the concentration of solution B was 5/6 $C_{B0}$ [$C_B$ = 2500 μm/(2500 + 500 μm) $C_{B0}$] for the red circled microreactor in Fig. 1.

Fig. S1 in the Supplementary Information shows a conceptual graph of the application of the support system we designed to overcome the difficulties of manually aligning matching holes, and the details were also introduced in the materials and methods section. Typically, this support system contained three parts: a plastic base, an outer square frame and a locator that possessed four cylinders with positions matched to those of the micropillars on the metal molds at the four corners. By locating the PDMS chip on the locator and pressing the locator inside the square frame with a silicon substrate or a PMMA block at the bottom on the plastic base, we could adhere the PDMS chip onto the silicon or PMMA block with a fixed position. The support system could also help ensure that the holes of the opposing PDMS chips were matched during the mixing and reaction process. The dark-red cylinder was a weight (500 g) used to ensure better contact and sealing effect between the PDMS chips.

### 3.1. High-throughput screening of the concentrations of reactants for calcium phosphates synthesis

To demonstrate the application of the designed screening platform, we investigated the synthesis of calcium phosphates micro/nanostructures because calcium phosphate is the prime inorganic mineral component in hard tissues of the human body, such as bones and teeth, and has been widely used as a biomedical material due to its properties of good biocompatibility, bioactivity and biodegradability. Calcium phosphates (CaP) micro/nanostructures were synthesized by a wet chemical precipitation process [22]; briefly, they were prepared by mixing a $Ca(NO_3)_2$ solution with an $(NH_4)_2HPO_4$ solution. We could obtain calcium phosphates micro/nanostructures with potentially different morphologies by screening the concentration ratio of different solutions using this platform.

As shown in Fig. 1, PDMS chip1 with partially perforated holes containing a 0.06 M $Ca(NO_3)_2$ solution was quickly flipped over in the right direction so that the deepest holes in PDMS chip1 aligned with the shallowest holes in PDMS chip2 and was placed on PDMS chip2, which held a 0.06 M $(NH_4)_2HPO_4$ solution. The reaction was triggered immediately after the two solutions came into contact, and the system was placed on a shaking table at 37 °C for 24 h. After reaction, the silicon substrate was washed and dried to obtain the desired CaP sediments. The silicon substrate with the samples was then coated with Pt for SEM scanning.

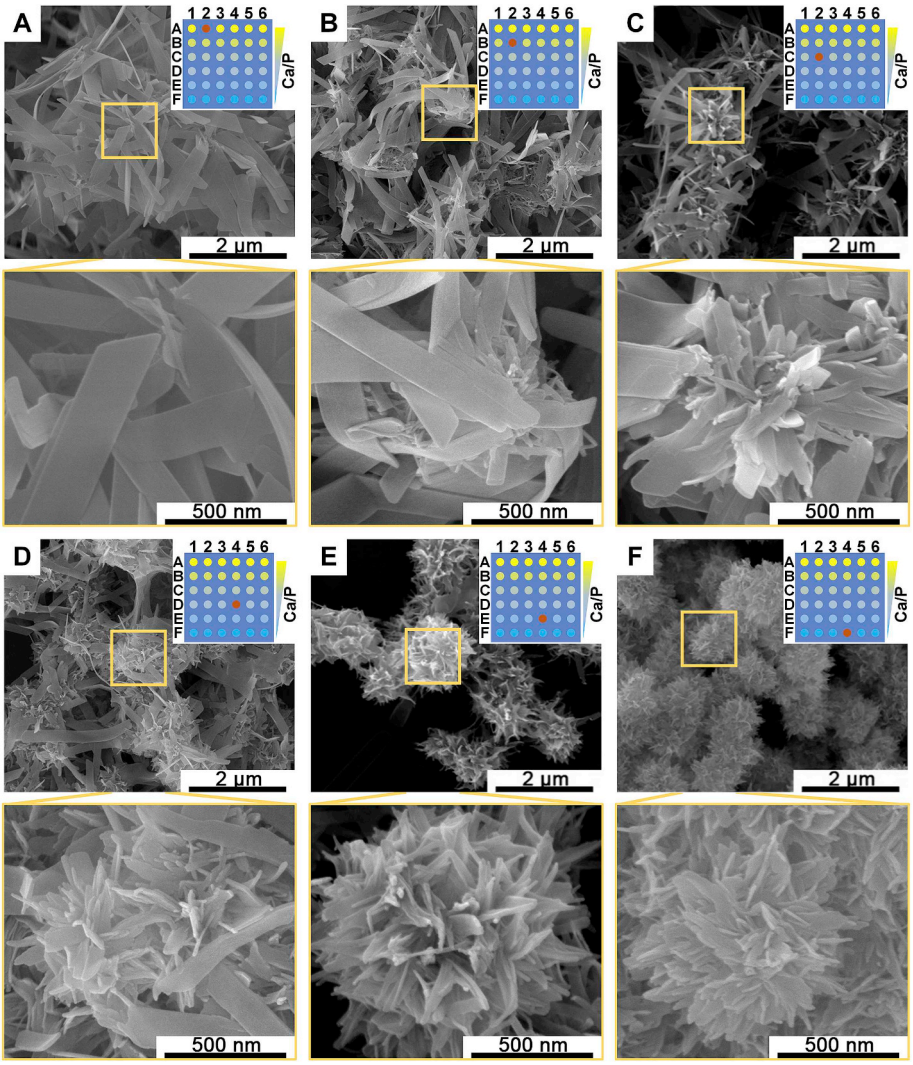


**Fig. 2.** SEM images of CaP structures for screening of the concentration ratio between two vital reactants [$Ca(NO_3)_2$ and $(NH_4)_2HPO_4$] with a gradient using the microarray platform: (**A**) $C_{Ca}/C_P$ = 2.5/0.5; (**B**) $C_{Ca}/C_P$ = 2.1/0.9; (**C**) $C_{Ca}/C_P$ = 1.7/1.3; (**D**) $C_{Ca}/C_P$ = 1.3/1.7; (**E**) $C_{Ca}/C_P$ = 0.9/2.1; (**F**) $C_{Ca}/C_P$ = 0.5/2.5.

Fig. 2 shows SEM images of the CaP structures synthesized by this microarray platform when screening the concentration ratio between two vital reactants [$Ca(NO_3)_2$ and $(NH_4)_2HPO_4$]. The concentration ratio of each microreactor was calculated following equation (1), and from Fig. 2A–F, the concentration ratio $C_{Ca}/C_P$ (=Ca/P, as the concentrations of solution $Ca(NO_3)_2$ and $(NH_4)_2HPO_4$ were both 0.06 M, the concentration ratio $C_{Ca}/C_P$ was equal to Ca/P molar ratio) was 2.5/0.5, 2.1/0.9, 1.7/1.3, 1.3/1.7, 0.9/2.1 and 0.5/2.5. As shown in Fig. 2, when the calcium concentration was relatively low, flower-like clusters (Fig. 2F) with a diameter of approximately 1 μm were generated, and the flower self-assembled structures were constituted by bunches of irregular and extremely thin flakes in all directions. The flower-like clusters became looser, the diameters of the clusters shrunk to micron-sized, and the flake unit also shrunk when the calcium concentration was increased. When $C_{Ca}/C_P$ was increased to 1.7/1.3, the assembled unit changed from irregular flakes to a strip structure. With a further increase of the calcium concentration, the flower-like clusters were covered by strip structures, and the width and aspect ratio of the strip structures significantly increased. When $C_{Ca}/C_P$ reached 5, the flower-like structures completely disappeared, and the main morphology of the CaP structure was a stack of wide (≈200 nm) and long (several microns) strips (Fig. 2A).

In the abovementioned experiment, we built a horizontal concentration ratio gradient of the two vital reactants ($C_{Ca}/C_P$ = 2.5/0.5; 2.1/0.9; 1.7/1.3; 1.3/1.7; 0.9/2.1; and 0.5/2.5). We also demonstrated an orthogonal $C_{Ca}/C_P$ concentration ratio gradient, as listed in Table 1. After adding 0.06 M $(NH_4)_2HPO_4$ to PDMS chip2 and 0.06 M $Ca(NO_3)_2$ solution to PDMS chip1, PDMS chip1 fixed on a PMMA block was quickly flipped over in a specific direction so that the end of PDMS chip1 with the deepest holes aligned with the deepest holes in PDMS chip2 and the other end of PDMS chip1 with the deepest holes aligned with the shallowest holes in PDMS chip2, and vice versa. Then, the PMMA block was pressed into the square frame. Except for the opposing PDMS chip alignment direction, the rest of the procedures were the same as in the preliminary experiment.

Fig. 3 shows SEM images of the CaP structures prepared through this microarray platform when screening the orthogonal concentration ratio gradient between two vital reactants [$Ca(NO_3)_2$ and $(NH_4)_2HPO_4$]. The concentration ratio of each microreactor was calculated and is listed in Table 1. It was obvious that when there was enough calcium component, the formed CaP structures had mainly long but extremely thin strip morphologies, usually several microns long and 200 nm wide; meanwhile, the width of the strip increased when more phosphate was added to the reaction. On the other hand, an increase in the phosphate component helped the CaP structure change from a needle-like structure to flower-like clusters when the calcium concentration was relatively low. Furthermore, for the relatively low phosphate concentration conditions, the needle-like structure gradually grew to a strip structure

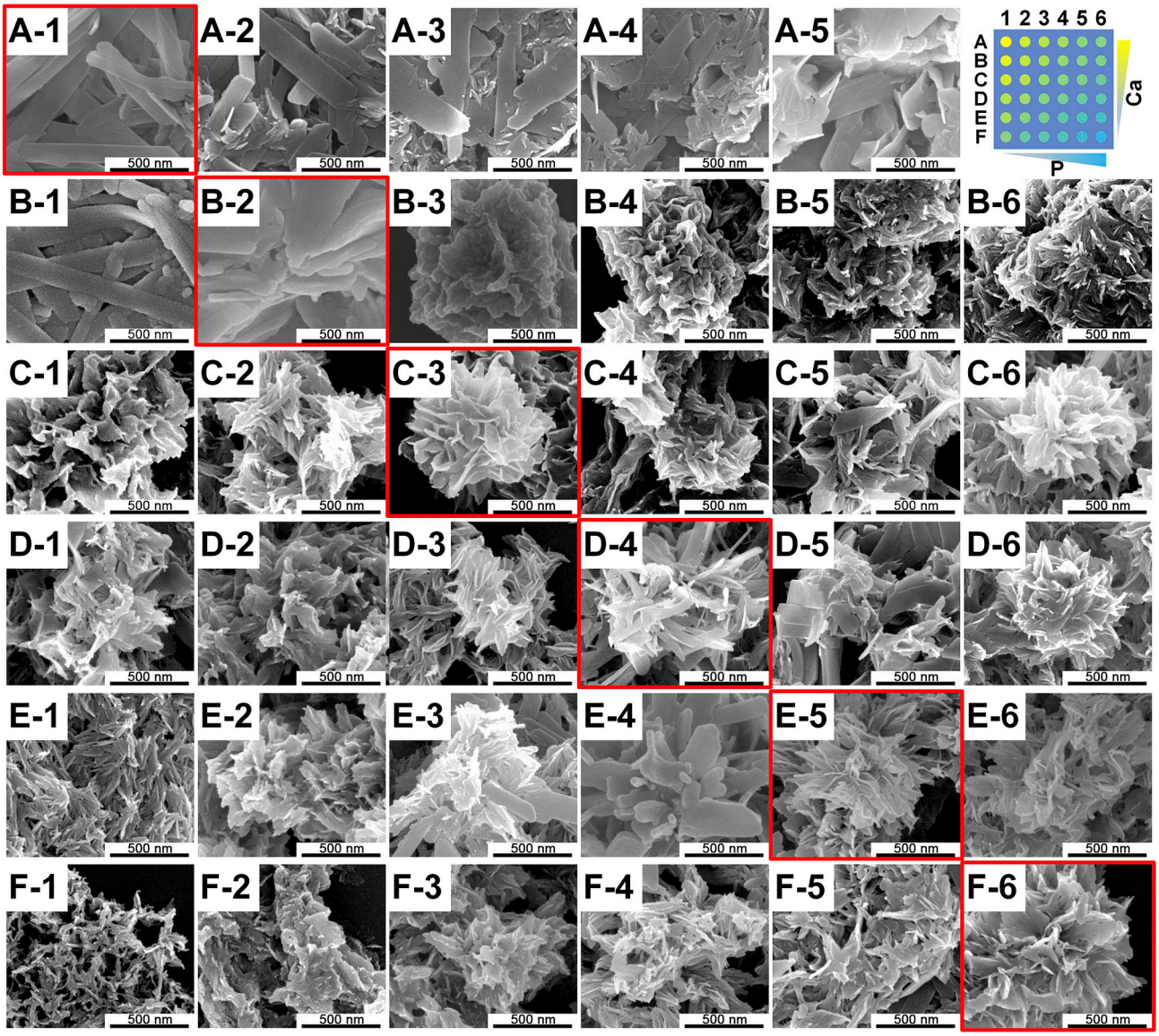


**Fig. 3.** SEM images of CaP structures for screening of the orthogonal concentration ratio between two vital reactants [$Ca(NO_3)_2$ and $(NH_4)_2HPO_4$] with a gradient using the microarray platform. The concentration ratio of each image is listed in Table 1 and is not listed here. The SEM images in the red box correspond to the CaP structures synthesized under the same conditions as in the horizontal experiments.

when the calcium concentration was increased. In addition, for the high phosphate concentration reactions, the increased calcium concentration led to flower-like clusters changing to strip structures.

### *3.2. Scale-up experiments for calcium phosphates synthesis according to screening results*

Based on the initial experimental conditions, we performed scale-up experiments, and the reaction volume was increased from $V_0$ = 2.355 μL to V = 15 μL ($V/V_0 \approx 6.37$). As the solvent inside the microreactor would continuously evaporate during the reaction, which would change the reaction dynamics, we took this into consideration, and in scale-up experiments, the concentrations of both reactants were increased by six times ($C_{Ca} = C_P = 0.36$ M). These scaled-up experiments were based on a rough estimation, and the parameters might be relatively effective for low volume conditions. However, for larger reaction volumes, the authors cannot ensure the validity. Briefly, $V_{Ca}$ μL of a 0.36 M $Ca(NO_3)_2$ solution was added into 0.5 mL EP tubes containing $V_P$ μL of a 0.36 M $(NH_4)_2HPO_4$ solution, and the volume ratio between the two solutions in each scale-up experiment was matched to the volume ratio between the two solutions in the chip screening experiment ($V_{Ca} + V_P$ = 15 μL: $V_{Ca1}$ = 12.5 μL, $V_{P1}$ = 2.5 μL, $V_{Ca1}/V_{P1}$ = 2.5/0.5; $V_{Ca2}$ = 10.5 μL, $V_{P2}$ = 4.5 μL, $V_{Ca2}/V_{P2}$ = 2.1/0.9; $V_{Ca3}$ = 8.5 μL, $V_{P3}$ = 6.5 μL, $V_{Ca3}/V_{P3}$ = 1.7/1.3; $V_{Ca4}$ = 6.5 μL, $V_{P4}$ = 8.5 μL, $V_{Ca4}/V_{P4}$ = 1.3/1.7; $V_{Ca5}$ = 4.5 μL, $V_{P5}$ = 10.5 μL, $V_{Ca5}/V_{P5}$ = 0.9/2.1; $V_{Ca6}$ = 2.5 μL, $V_{P6}$ = 12.5 μL, $V_{Ca6}/V_{P6}$ = 0.5/2.5). The reaction tubes were placed on a shaking table at 37 °C for 24 h, after which the supernatant liquid in the EP tubes was removed. The precipitates were washed and dispersed by deionized water, then dripped on filter paper to remove soluble impurities and air dried. The dried precipitates were collected for SEM and other characterization.

As demonstrated in Fig. 4, when $C_{Ca}/C_P$ = 0.5/2.5, flower-like clusters with a diameter of approximately 1 μm composed of nanoscale irregular flakes were observed. The density and diameter of the clusters were both reduced but the flake unit became thicker when the calcium concentration was increased. When $C_{Ca}/C_P$ rose to 1.7/1.3, significant differences appeared; the nanosized flake unit was increased to the micron order, and there was still a growth core. With further increases in $C_{Ca}/C_P$, the flower-like core dissipated, and the width and aspect ratio of the strips significantly increased. When $C_{Ca}/C_P$ reached 2.5/0.5,

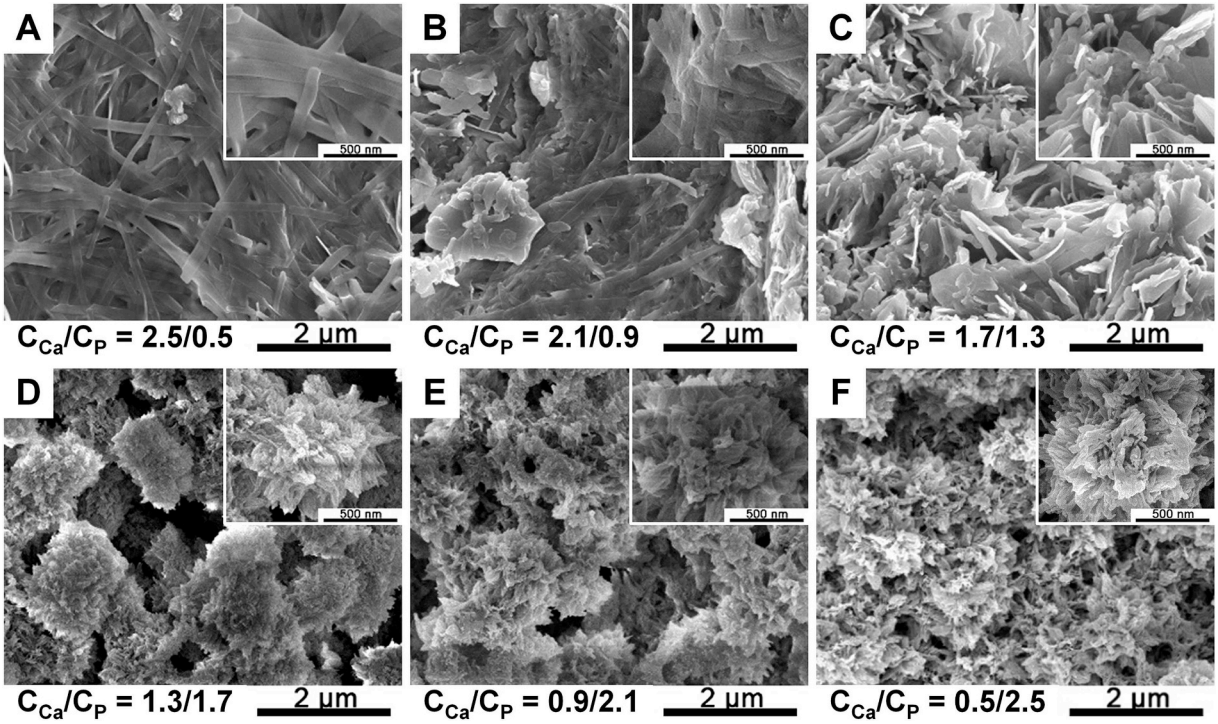


**Fig. 4.** Scale-up experiments. SEM images of CaP structures synthesized in EP tubes. (**A**) $C_{Ca}/C_P$ = 2.5/0.5; (**B**) $C_{Ca}/C_P$ = 2.1/0.9; (**C**) $C_{Ca}/C_P$ = 1.7/1.3; (**D**) $C_{Ca}/C_P$ = 1.3/1.7; (**E**) $C_{Ca}/C_P$ = 0.9/2.1; (**F**) $C_{Ca}/C_P$ = 0.5/2.5.

the flower-like structure was completely replaced by a stack of wide strip structures. It was worth mentioning that the morphologies of CaP synthesized in scale-up experiments matched with the microarray screening which confirmed the practicability, accuracy and reliability of our platform.

Fig. S3 in the Supplementary Information provides the XRD results of CaP prepared in the scale-up experiments and microarray platform. When $C_{Ca}/C_P$ < 1.3/1.7, the characteristic peaks representing the apatite phase could be readily identified in both the scale-up and screening experiments. Meanwhile, the XRD patterns of CaP synthesized with relatively high $C_{Ca}/C_P$ suggested that the formed CaP possessed the brushite (dicalcium phosphate dihydrate, DCPD, $CaHPO_4{\cdot}2H_2O$) crystal structure. In addition, the CaP generated when $C_{Ca}/C_P$ = 1.3/1.7 was a mixture of both apatite and brushite, as both materials' characteristic peaks were observed in the XRD pattern in the scale-up experiment. The consistency of XRD results amongst both microarray platform and the scale-up experiments suggested the fidelity and reliability of designed platform. The Fourier transform-infrared (FT-IR) spectra of CaP samples synthesized in the scale-up experiments are shown in Fig. S4 in the Supplementary Information. The spectra of all samples showed specific absorption peaks of calcium phosphates, at 1033, 602, and 565 $cm^{-1}$. When $C_{Ca}/C_P$ was relatively high (> 1.3/1.7), a peak at 2390 $cm^{-1}$ was observed in the FT-IR spectra, which indicated the existence of the brushite structure.

### 3.3. High-throughput screening the concentration of additive reagent for calcium phosphates synthesis

To introduce multiple reagents into the research, we also designed another metal mold to fabricate PDMS chip3 and chip4, in which the holes had a uniform depth (1500 μm). Fig. 5 shows a schematic of the procedure for the application of this platform to other agent (*i.e.*, additives) concentration screening. Briefly, PDMS chip1 containing a cylindrical hole array with a depth gradient (the depth of the holes in each column were 500, 900, 1300, 1700, 2100 and 2500 μm and in each row were the same) and PDMS chip3 containing an array of cylindrical holes with the same depth (1500 μm) were combined. PDMS chip1 contained solution A ($C_A$), while PDMS chip3 contained a mixed solution of A and C ($C_A$; $C_{C0}$). Then, PDMS chip1 was quickly flipped over and placed on PDMS chip3. Upon mixing of the solutions in the matched holes for 2 h to ensure complete diffusion between the solutions, after peeling off PDMS chip1, the holes in PDMS chip3 contained a mixed solution with solution A ($C_A$) and a solution C ($C_{C-}$) gradient. Then, PDMS chip3 was quickly flipped over and placed on PDMS chip4 containing solution B ($C_B$) fixed on a silicon substrate. Upon mixing of the solutions in the matched holes, the reaction was triggered immediately after the two solutions came into contact. After the reaction, the precipitated target product was found on the silicon substrate at the corresponding microreactor position, which means that we could obtain a product array for SEM and other characterization. Furthermore, the additive reagent concentration could be determined by calculation according to the equation below:

$$C_X = d_X / (d_X + d_A) \times C_{X0} \quad (2)$$

$C_X$ is the solution concentration of additive reagent X in the microreactor; $d_X$ is the depth of the holes in PDMS chip1 containing solution X, $d_A$ (= 1500 μm) is the depth of the holes in PDMS chip3 containing solution A, and $C_{x0}$ is the concentration of solution X initially added into PDMS chip1. For instance, the concentration of solution C was 5/8 $C_{C0}$ [$C_C$ = 2500 μm/(2500 + 1500 μm) $C_{C0}$] for the red circled well in Fig. 5.

To demonstrate the function of the designed screening platform, we focused on the influence of the NaOH concentration on the synthesis of calcium phosphates micro/nanostructures. As shown in Fig. 5, PDMS chip3 with partially perforated holes containing a 0.06 M $Ca(NO_3)_2$ solution (pH adjusted to 4.51) was quickly flipped over and placed on PDMS chip1, which held a mixed solution of 0.06 M $(NH_4)_2HPO_4$ and 0.070 M NaOH. Upon mixing of the solutions in matched holes for 2 h to ensure complete diffusion, after peeling off PDMS chip1, the holes in PDMS chip3 contained a mixed solution with 0.06 M $(NH_4)_2HPO_4$ and a NaOH concentration gradient (0.0175, 0.0263, 0.0325, 0.0372, 0.0408 and 0.0438 M). Then, PDMS chip3 was quickly flipped over and placed

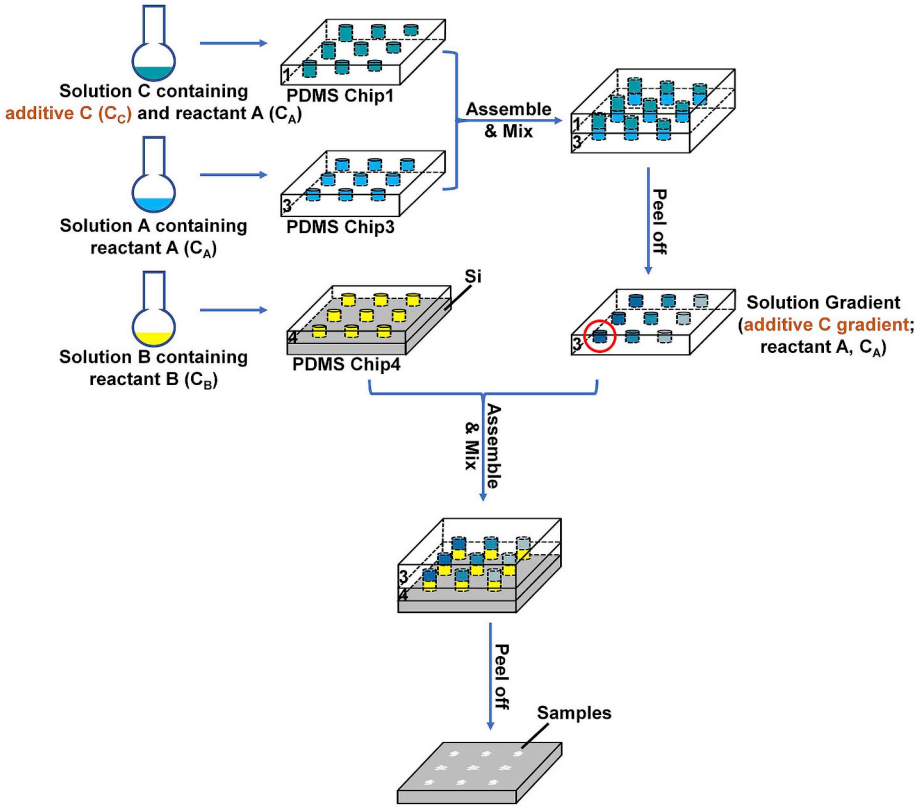


**Fig. 5.** Schematic overview of fabricating microreactors on a silicon substrate: PDMS chip1 and PDMS chip3 with partially perforated holes; a reactant solution was added into PDMS chip3, while a mixed solution of this reactant with the same concentration and an additive reagent was added into PDMS chip1; then, the PDMS chip1 was placed on PDMS chip3 to mix the solutions in the wells, and PDMS chip3 was reserved after mixing; PDMS chip4 with fully perforated holes containing the other reactant fixed on a silicon substrate and PDMS chip3 was placed on PDMS chip4 to mix the solutions in the wells, and the reaction was initiated after mixing; a precipitated product array could be found on the silicon substrate after reaction.

on PDMS chip4 containing a 0.10 M $Ca(NO_3)_2$ solution fixed on a silicon substrate. The reaction was triggered when the two solutions came into contact, and the system was placed on a shaking table at 37 ˚C for 24 h. After reaction, the silicon substrate was washed and dried to obtain the desired CaP sediments. The silicon substrate with the samples was then coated with Pt for SEM scanning. To expand the research, another NaOH concentration gradient was built by adding a 0.06 M $(NH_4)_2HPO_4$ solution (pH adjusted to 7.00) to PDMS chip3, while a mixed solution contained 0.06 M $(NH_4)_2HPO_4$ and 0.225 M NaOH was added into PDMS chip1, and a small NaOH concentration gradient (0.0563, 0.0844, 0.1045, 0.1195, 0.1313 and 0.1406 M) was generated. The remaining procedures remained the same as before. The SEM results are shown in Fig. 6, and the NaOH concentration and pH of the mixed 0.06 M $(NH_4)_2HPO_4$ and NaOH solution in PDMS chip3 before reaction are listed in Table 2.

As observed in Fig. 6, when a high amount of NaOH was added into the reaction system, the formed CaP exhibited a flower-like structure, and the morphology changed slightly when more NaOH was introduced into the reaction. For instance, the density and diameter of the flower clusters both increased when more NaOH was involved. When the acidic phosphate solution was mixed with NaOH, the flower-like structure shrunk to a porous spherical structure, and the diameter of the spheres decreased while the pores inside them increased and the spheres eventually disaggregated in weakly alkaline to neutral environments.

## 4. Discussion

The colorant mixing experiment showed that this microarray platform could generate a stable concentration gradient. As shown in Fig. S2 in the Supplementary Information, a clear color changing gradient was presented; from left to right, the color of the microreactors ranged from dark cyan to deep green and ultimately a pale green tone since the microreactors in the upper PDMS chip1 contained a brilliant blue pigment whose concentration was reduced from left to right, while the situation of PDMS chip2 below was the exact opposite. Additionally, the color change was intensified by the contrast between it and a piece of white filter paper under PDMS chip1 (Fig. S2 in the Supplementary Information), and it was also notable that the solution color only changed in the horizontal direction, while in the vertical direction, the color in each column remained consistent. This suggested that the formed concentration gradient was reliable and stable.

The morphology of the CaP structures obtained in the microarray platform (Fig. 2) and EP tubes (Fig. 4) under the same conditions showed a certain uniformity. Flower-like structures were obtained under low Ca/P conditions and changed to long strip structures with increasing Ca/P. The details might be slightly different; however, the overall morphological change trends matched, which confirmed the dependability and practicability of the designed screening platform.

The consistency of XRD results amongst both microarray platform and the scale-up experiments also suggested the fidelity and reliability of designed platform. The changing point of the CaP morphology in both Figs. 2 and 4 was at Ca/P = 1.7/1.3, which also matched the XRD results of the samples synthesized in the scale-up experiments and the platform. The XRD patterns of the samples formed under low Ca/P conditions showed some characteristic peaks of apatite, such as the reflection peak at 25˚–27˚ corresponding to the 002 plane and broad peak at 30˚–35˚ corresponding to the 211 + 300 planes [23–25]. This helped prove the former conclusion that the main phase of the Ca/P samples synthesized in low Ca/P conditions can be indexed to apatite. In addition, for brushite, XRD reflection peaks at 11.6˚, corresponding to the 020 plane, 23.6˚, corresponding to the 040 plane, and 29.3˚, corresponding to the 112 plane, were observed [26,27]. When Ca/P = 1.3/1.7, the XRD pattern showed the characteristic peaks of the apatite and brushite structures, and when Ca/P was increased to 1.7/1.3, only brushite peaks were found in the XRD pattern. This was also the reaction condition when the peak at 2390 $cm^{-1}$ was observed in the FT-IR spectrum, and the peak at 2390 $cm^{-1}$ was caused by O–H internal bending vibration in the $HPO4^{2-}$ group [28], indicating the existence of brushite.

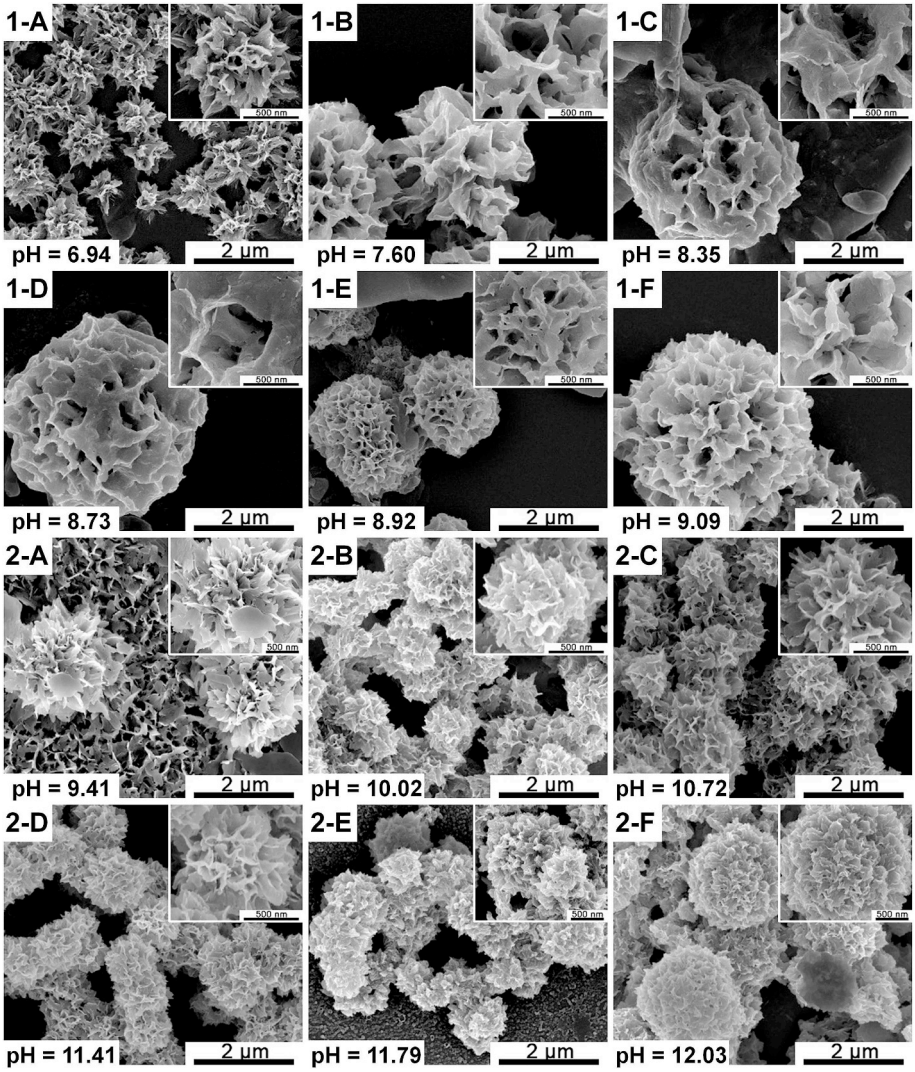


**Fig. 6.** SEM images of CaP structures synthesized in the microarray platform for screening of a NaOH concentration gradient. (**1-A**) to (**1-F**): $C_P$ = 0.06 M and $pH_{01}$ = 4.51 in PDMS chip3 with $C_P$ = 0.06 M and $C_{NaOH}$ = 0.070 M in PDMS chip1; from A to F, the depths of the holes in PDMS chip1 varied from low to high; (**2-A**) to (**2-F**) $C_P$ = 0.06 M and $pH_{02}$ = 7.00 in PDMS chip3 with $C_P$ = 0.06 M and $C_{NaOH}$ = 0.225 M PDMS chip1; from A to F, the depths of the holes in PDMS chip1 varied from low to high.

The morphology and crystal structure changes were driven by the reaction kinetics. The CaP salt system contained apatite, tribasic calcium phosphate (TCP), crystalline octacalcium phosphate (OCP), dicalcium phosphate dihydrate (DCPD, aka brushite), etc. [27,29]. Therefore, during the crystallization process, the concentrations of $Ca^{2+}$, $PO_4^{3-}$ and pH ($OH^-$) could influence the crystalline phase transition because a concentration change could affect the degree of supersaturation, and an increased supersaturation degree would lead to nucleation and crystal growth [25,30,31]. The final morphology of the crystal was determined by the anisotropy of the individual crystal plane growth rates [32,33]. This

**Table 2**
NaOH concentration and pH of the mixed 0.06 M $(NH_4)_2HPO_4$ and NaOH solution in PDMS chip3 for reaction.

| | PDMS chip1 | Depth (mm) | PDMS chip3 | Depth (mm) | NaOH concentration (M) in mixed PDMS chip3 | pH of mixed PDMS chip3 |
|---|---|---|---|---|---|---|
| 1-A | 0.06 M $(NH_4)_2$ | 0.5 | 0.06 M | 1.5 | 0.0175 | 6.94 |
| 1-B | $HPO_4$/0.070 M NaOH | 0.9 | $(NH_4)_2HPO_4$ | | 0.0263 | 7.60 |
| 1-C | | 1.3 | pH = 4.51 | | 0.0325 | 8.35 |
| 1-D | | 1.7 | | | 0.0372 | 8.73 |
| 1-E | | 2.1 | | | 0.0408 | 8.92 |
| 1-F | | 2.5 | | | 0.0438 | 9.09 |
| 2-A | 0.06 M $(NH_4)_2$ | 0.5 | 0.06 M | 1.5 | 0.0563 | 9.41 |
| 2-B | $HPO_4$/0.225 M NaOH | 0.9 | $(NH_4)_2HPO_4$ | | 0.0844 | 10.02 |
| 2-C | | 1.3 | pH = 7.00 | | 0.1045 | 10.72 |
| 2-D | | 1.7 | | | 0.1195 | 11.41 |
| 2-E | | 2.1 | | | 0.1313 | 11.79 |
| 2-F | | 2.5 | | | 0.1406 | 12.03 |

system contained Ca–$P_6O_{24}$ (*c* axis) and $OH^-$-$Ca^{2+}$ (*a*, *b* axes). The Ca–$P_6O_{24+}$ complex anion was relatively stable as a result of the CaP crystal growing along the *c* axis, and a strip-like structure was formed [34,35]. On the other hand, $(NH_4)_2HPO_4$ solution is an alkaline solution; thus, there would be more $OH^-$ in the system, which would generate $OH^-$-$Ca^{2+}$, and the crystal would also grow along the *a* and *b* axes [35]. This was the reason why flower-like and sphere structures tended to form at increased $(NH_4)_2HPO_4$ solution concentration and NaOH concentration.

## 5. Conclusions

We presented a microarray platform and parallel experiments with similar reaction conditions can be carried out on this platform synthesizing a series of aiming samples in a single experiment. By generating gradient of interest parameter, range of conditions to obtain different product morphologies could be quickly identified. Different phases of micro/nanosized calcium phosphates structures with diverse morphologies were synthesized when the experimental conditions (*i.e.*, reaction concentration, pH) were screened on our platform. The morphologies of CaP particles were strongly influenced by the Ca/P concentration ratio and NaOH concentration. And the scale-up experiments proved the practicability, accuracy and reliability of the microarray platform. This technique is expected to accelerate the research process, optimize the reactive conditions and provide mass data for future machine learning. This is a universal technique and is also expected to apply to other systems for high-throughput screening of reaction conditions related to the production of various structure.

## CRediT authorship contribution statement

**Xiaoyu Li:** Conceptualization, Methodology, Validation, Formal analysis, Investigation, Data curation, Writing - original draft, Writing - review & editing. **Xiran Yang:** Validation, Formal analysis, Investigation, Data curation, Writing - review & editing. **Lei Liu:** Validation, Formal analysis, Writing - review & editing. **Peipei Zhou:** Validation, Methodology, Writing - review & editing. **Jianhua Zhou:** Supervision, Resources, Writing - review & editing, Funding acquisition. **Xuetao Shi:** Supervision, Resources, Writing - review & editing, Project administration, Funding acquisition. **Yingjun Wang:** Supervision, Resources, Project administration, Funding acquisition.

## Declaration of competing interest

The authors declare no conflict of interest.

## Acknowledgments

This work was financially supported by the Science and Technology Program of Guangdong Province (2019B010941002, 2017B090911008, 2016A030306018), the National Natural Science Foundation of China (No.51905557) and Outstanding Scholar Program of Guangzhou Regenerative Medicine and Health Guangdong Laboratory (2018GZR110102001).

## Appendix A. Supplementary data

Supplementary data to this article can be found online at https://doi.org/10.1016/j.bioactmat.2020.02.003.

## Abbreviations

| | |
|---|---|
| CaP | Calcium Phosphates |
| Ca/P | Ca/P Molar Ratio |
| FE-SEM | Field Emission Scanning Electron Microscope |
| FT-IR | Fourier Transform-Infrared |
| XRD | X-ray Diffraction |

## References

[1] A. Jain, S.P. Ong, G. Hautier, W. Chen, W.D. Richards, S. Dacek, S. Cholia, D. Gunter, D. Skinner, G. Ceder, K.A. Persson, Commentary: the Materials Project: a materials genome approach to accelerating materials innovation, Apl. Mater. 1 (2013) e011002, , https://doi.org/10.1063/1.4812323.
[2] Y. Lan, X. Han, M. Tong, H. Huang, Q. Yang, D. Liu, X. Zhao, C. Zhong, Materials genomics methods for high-throughput construction of COFs and targeted synthesis, Nat. Commun. 9 (2018) e5274, , https://doi.org/10.1038/s41467-018-07720-x.
[3] L.G. Otten, F. Hollmann, I.W.C.E. Arends, Enzyme engineering for enantioselectivity: from trial-and-error to rational design? Trends Biotechnol. 28 (2010) 46–54, https://doi.org/10.1016/j.tibtech.2009.10.001.
[4] R. Potyrailo, K. Rajan, K. Stoewe, I. Takeuchi, B. Chisholm, H. Lam, Combinatorial and high-throughput screening of materials libraries: review of state of the art, ACS Comb. Sci. 13 (2011) 579–633, https://doi.org/10.1021/co200007w.
[5] M.A. Al-Sayah, P. Rizos, V. Antonucci, N. Wu, High throughput screening of active pharmaceutical ingredients by UPLC, J. Separ. Sci. 31 (2008) 2167–2172, https://doi.org/10.1002/jssc.200700594.
[6] A. Andrade-Eiroa, R. Shahla, M.N. Romanías, P. Dagaut, An alternative to trial and error methodology in solid phase extraction: an original automated solid phase extraction procedure for analysing PAHs and PAH-derivatives in soot, RSC Adv. 4 (2014) 33636–33644, https://doi.org/10.1039/c4ra03214d.
[7] D.P. Tabor, L.M. Roch, S.K. Saikin, C. Kreisbeck, D. Sheberla, J.H. Montoya, S. Dwaraknath, M. Aykol, C. Ortiz, H. Tribukait, C. Amador-Bedolla, C.J. Brabec, B. Maruyama, K.A. Persson, A. Aspuru-Guzik, Accelerating the discovery of materials for clean energy in the era of smart automation, Nat. Rev. Mater. 3 (2018) 5–20, https://doi.org/10.1038/s41578-018-0005-z.
[8] K. Alberi, M.B. Nardelli, A. Zakutayev, L. Mitas, S. Curtarolo, A. Jain, M. Fornari, N. Marzari, I. Takeuchi, M.L. Green, M. Kanatzidis, M.F. Toney, S. Butenko, B. Meredig, S. Lany, U. Kattner, A. Davydov, E.S. Toberer, V. Stevanovic, A. Walsh, N.-G. Park, A. Aspuru-Guzik, D.P. Tabor, J. Nelson, J. Murphy, A. Setlur, J. Gregoire, H. Li, R. Xiao, A. Ludwig, L.W. Martin, A.M. Rappe, S.-H. Wei, J. Perkins, The 2019 materials by design roadmap, J. Phys. D Appl. Phys. 52 (2019) e013001, , https://doi.org/10.1088/1361-6463/aad926.
[9] E.A. Pfeif, K. Kroenlein, Perspective: data infrastructure for high throughput materials discovery, Apl. Mater. 4 (2016) e053203, , https://doi.org/10.1063/1.4942634.
[10] A.B. Santanilla, E.L. Regalado, T. Pereira, M. Shevlin, K. Bateman, L.-C. Campeau, J. Schneeweis, S. Berritt, Z.-C. Shi, P. Nantermet, Y. Liu, R. Helmy, C.J. Welch, P. Vachal, I.W. Davies, T. Cernak, S.D. Dreher, Nanomole-scale high-throughput chemistry for the synthesis of complex molecules, Science 347 (2015) 49–53, https://doi.org/10.1126/science.1259203.
[11] D. Perera, J.W. Tucker, S. Brahmbhatt, C.J. Helal, A. Chong, W. Farrell, P. Richardson, N.W. Sach, A platform for automated nanomole-scale reaction screening and micromole-scale synthesis in flow, Science 359 (2018) 429–434, https://doi.org/10.1126/science.aap9112.
[12] A.K. Price, A.B. MacConnell, B.M. Paegel, *h*νSABR: photochemical dose–response bead screening in droplets, Anal. Chem. 88 (2016) 2904–2911, https://doi.org/10.1021/acs.analchem.5b04811.
[13] A.B. Theberge, F. Courtois, Y. Schaerli, M. Fischlechner, C. Abell, F. Hollfelder, W.T.S. Huck, Microdroplets in microfluidics: an evolving platform for discoveries in chemistry and biology, Angew. Chem. Int. Ed. 49 (2010) 5846–5868, https://doi.org/10.1002/anie.200906653.
[14] D.T. Chiu, A.J. deMello, D.D. Carlo, P.S. Doyle, C. Hansen, R.M. Maceiczyk, R.C.R. Wootton, Small but perfectly formed? Successes, challenges, and opportunities for microfluidics in the chemical and biological sciences, Inside Chem. 2 (2017) 201–223, https://doi.org/10.1016/j.chempr.2017.01.009.
[15] M. Funke, A. Buchenauer, U. Schnakenberg, W. Mokwa, S. Diederichs, A. Mertens, C. Müller, F. Kensy, J. Büchs, Microfluidic biolector-microfluidic bioprocess control in microtiter plates, Biotechnol. Bioeng. 107 (2010) 497–505, https://doi.org/10.1002/bit.22825.
[16] D. Witters, N. Vergauwe, R. Ameloot, S. Vermeir, D.D. Vos, R. Puers, B. Sels, J. Lammertyn, Digital microfluidic high-throughput printing of single metal-organic framework crystals, Adv. Mater. 24 (2012) 1316–1320, https://doi.org/10.1002/adma.201104922.
[17] E.K. Sackmann, A.L. Fulton, D.J. Beebe, The present and future role of microfluidics in biomedical research, Nature 507 (2014) 181–189, https://doi.org/10.1038/nature13118.
[18] J. Zhou, J. Zeng, J. Grant, H. Wu, Y. Xia, On-chip screening of experimental conditions for the synthesis of noble-metal nanostructures with different morphologies, Small 7 (2011) 3308–3316, https://doi.org/10.1002/smll.201101299.
[19] S.V. Dorozhkin, E. Matthias, Biological and medical significance of calcium phosphates, Angew. Chem. Int. Ed. 41 (2002) 3130–3146.
[20] H.H. Xu, P. Wang, L. Wang, C. Bao, Q. Chen, M.D. Weir, L.C. Chow, L. Zhao, X. Zhou, M.A. Reynolds, Calcium phosphate cements for bone engineering and their biological properties, Bone Res. 5 (2017) e17056, , https://doi.org/10.1038/boneres.2017.56.
[21] N. Eliaz, N. Metoki, Calcium phosphate bioceramics: a review of their history, structure, properties, coating technologies and biomedical applications, Materials 10 (2017) e334, https://doi.org/10.3390/ma10040334.
[22] K. Salma, L. Berzina-Cimdina, N. Borodajenko, Calcium phosphate bioceramics prepared from wet chemically precipitated powders, Process. Appl. Ceram. 4 (2010) 45–51, https://doi.org/10.2298/PAC1001045S.
[23] A. Ślósarczyk, Z. Paszkiewicz, C. Paluszkiewicz, FTIR and XRD evaluation of carbonated hydroxyapatite powders synthesized by wet methods, J. Mol. Struct.

744–747 (2005) 657–661, https://doi.org/10.1016/j.molstruc.2004.11.078.
[24] S.N. Danilchenko, A.N. Kalinkevich, R.A. Moskalenko, V.N. Kuznetsov, A.V. Kochenko, E.V. Husak, V.V. Starikov, F. Liu, J. Meng, J. Lü, Structural and crystal-chemical characteristics of the apatite deposits from human aortic walls, Interv. Med. Appl. Sci. 10 (2018) 110–119, https://doi.org/10.1556/1646.10.2018.24.
[25] C. Drouet, Apatite formation: why it may not work as planned, and how to conclusively identify apatite compounds, BioMed Res. Int. 2013 (2013) e490946, , https://doi.org/10.1155/2013/490946.
[26] S.M. Arifuzzaman, S. Rohani, Experimental study of brushite precipitation, J. Cryst. Growth 267 (2004) 624–634, https://doi.org/10.1016/j.jcrysgro.2004.04.024.
[27] T. Toshima, R. Hamai, M. Tafu, Y. Takemura, S. Fujita, T. Chohji, S. Tanda, S. Li, G.W. Qin, Morphology control of brushite prepared by aqueous solution synthesis, J. Asian Ceram. Soc. 2 (2014) 52–56, https://doi.org/10.1016/j.jascer.2014.01.004.
[28] L. BerzinaCimdina, N. Borodajenko, Research of calcium phosphates using Fourier transform infrared spectroscopy, in: T. Theophanides (Ed.), Infrared Spectroscopy - Materials Science, Engineering and Technology, InTech, Croatia, 2012, pp. 123–148.
[29] X. Liu, J. Wang, Impact of calcium on struvite crystallization in the wastewater and its competition with magnesium, Chem. Eng. J. 378 (2019) e122121, , https://doi.org/10.1016/j.cej.2019.122121.
[30] S. Lee, H.S. Wi, W. Jo, Y.C. Cho, H.H. Lee, S.-Y. Jeong, Y.-I. Kim, G.W. Lee, Multiple pathways of crystal nucleation in an extremely supersaturated aqueous potassium dihydrogen phosphate (KDP) solution droplet, Proc. Natl. Acad. Sci. Unit. States Am. 113 (2016) 13618–13623, https://doi.org/10.1073/pnas.1604938113.
[31] P.G. Vekilov, Nucleation, Cryst. Growth Des. 10 (2010) 5007–5019, https://doi.org/10.1021/cg1011633.
[32] I. Rosbottom, C.Y. Ma, T.D. Turner, R.A. O'Connell, J. Loughrey, G. Sadiq, R.J. Davey, K.J. Roberts, Influence of solvent composition on the crystal morphology and structure of *p*-aminobenzoic acid crystallized from mixed ethanol and nitromethane solutions, Cryst. Growth Des. 17 (2017) 4151–4161, https://doi.org/10.1021/acs.cgd.7b00425.
[33] Y. Yang, S. Xu, M. Xie, Y. He, G. Huang, Y. Yang, Growth mechanisms for spherical mixed hydroxide agglomerates prepared by co-precipitation method: a case of $Ni_{1/3}Co_{1/3}Mn_{1/3}(OH)_2$, J. Alloys Compd. 619 (2015) 846–853, https://doi.org/10.1016/j.jallcom.2014.08.152.
[34] Y. Zhu, L. Xu, C. Liu, C. Zhang, N. Wu, Nucleation and growth of hydroxyapatite nanocrystals by hydrothermal method, AIP Adv. 8 (2018) e085221, , https://doi.org/10.1063/1.5034441.
[35] P. Wang, C. Li, H. Gong, X. Jiang, H. Wang, K. Li, Effects of synthesis conditions on the morphology of hydroxyapatite nanoparticles produced by wet chemical process, Powder Technol. 203 (2010) 315–321, https://doi.org/10.1016/j.powtec.2010.05.023.